



## Effects of rGO Concentration on Electrical and Mechanical Properties of rGO Natural Rubber Nanocomposite

D.N.P.I. CHATHURANGA<sup>1,2</sup>, R.C.L DE SILVA<sup>1</sup>, L.D.C NAYANAJITH<sup>1</sup>, A.M.K.L. ABEYKOON<sup>1</sup>, H.C.D.P COLOMBAGE<sup>1</sup>, M.H.T. DULAJ<sup>1</sup> and I.R.M KOTTEGODA<sup>1</sup>

<sup>1</sup>Materials Technology Section of Industrial Technology Institute,  
No. 363, Bauddhaloka Mawatha, Colombo 07, Sri Lanka.

<sup>2</sup>Department of Physics, University of Sri Jayewardenepura,  
Gangodawila, Nugegoda, Sri Lanka.

### Abstract

Nanocomposites of natural rubber (NR) with reduced graphene oxide (rGO) were prepared by varying their ratios intending to improve the electrical and mechanical properties of natural rubber. rGO was prepared through oxidation and subsequent reduction of high purity Sri Lankan vein graphite. The prepared nanocomposites were characterized using Fourier transform infrared spectroscopy (FTIR), scanning electron microscopy (SEM), and X-ray diffraction (XRD) techniques. The SEM images viewed a uniform homogeneous surface of the nanocomposite while FTIR and XRD spectral signatures substantiated its chemical functionalities and structural traits respectively. Mechanical properties such as tensile stress & strain, elongation at break, hardness, Young's modulus, and strain of the nanocomposite, were also investigated. Here the electrical conductivity was measured using the two-probe method. The nanocomposite started conducting at 2% rGO in rubber and increased conducting with increasing rGO. The hardness of the composites continuously increased with increasing rGO in rubber. Despite the tensile strength and elongation at break, Young's modulus also increased with increasing the rGO percentage up to 1.5 % and was optimized at the particular ratio. The highest strength of 15.91MPa was obtained at 1.5% of rGO. A detailed property investigation of rGO/NR nanocomposite has not been reported previously for the best of our knowledge. Hence, the study expected to be well supportive for future industrial developments including electronics, electrical devices, batteries, capacitors, as well as in heavy equipment including aerospace and automobiles.



### Article History

Received: 08 June 2023

Accepted: 21 July 2023

### Keywords

FTIR;  
Natural Rubber;  
Reduced Graphene  
Oxide rGO;  
SEM;  
XRD.

**CONTACT** D.N.P.I. Chaturanga ✉ imantha.dnp@gmail.com 📍 Materials Technology Section of Industrial Technology Institute, No. 363, Bauddhaloka Mawatha, Colombo 07, Sri Lanka.



© 2023 The Author(s). Published by Enviro Research Publishers.

This is an Open Access article licensed under a Creative Commons license: Attribution 4.0 International (CC-BY).

Doi: <http://dx.doi.org/10.13005/msri/200203>

## Introduction

Rubber is a widely recognized polymer that possesses exceptional properties such as superior abrasion resistance, tear resistance, elongation, flexibility, and resilience. Natural rubber products are typically categorized as dry rubber and latex based products.<sup>1</sup> Besides, NR has excellent dynamic properties, significant building track, and low-heat building-up.<sup>2</sup> Techniques such as coating, casting, extrusion, foaming, molding, and dipping are commonly used for manufacturing industrial and consumer products from NR latex. Due to these remarkable properties, NR based productions are utilized in many industries such as automobile, mechanical engineering, sport, apparel, medical, household, and consumer applications.<sup>1,3</sup> Most of the world's rubber production is used to manufacture tires and related products such as tubes, tire flaps, pneumatic tires, solid tires, retread material, puncture repair kits, etc. NR is further used to manufacture seals and various forms of padding for many automobile parts, such as brake pads, windows/ windshield seals, airbags, etc. In addition, they are used to manufacture gaskets, nozzles, conveyer belts, "O" – rings, vibrations, soundproof materials, etc.

Fillers are extensively useful in industries such as rubber and thermoplastic industries to enhance the tensile strength, modulus, tear resistance, abrasion resistance, and dynamic mechanical properties. Usually, these fillers contribute to the variation in the dynamic and mechanical properties of the product. Furthermore, these fillers change the production volume and mass, reducing the cost of production. As a result, fillers are economically crucial in NR-related production. However, the properties such as low modulus and strength restrict the rubber applications in significant applications.<sup>4</sup> Therefore, it is essential to choose appropriate fillers to achieve essential properties in each industrial application.

Graphene is a special material which consist of a higher amount of extraordinary qualities, such as greater flexibility, strength, lightweight, and electrical/ thermal conductivity. Reduced graphene oxide (rGO) and graphene oxide (rGO) are the main cost-effective graphene materials broadly applicable in many fields.<sup>4</sup> Due to the molecular similarity to graphene and lower cost than graphene, rGO is receiving a significant attention among the

scientific community.<sup>5</sup> The integration of rGO with conventional materials to create composite materials is extensively utilized in various industries owing to its straightforward implementation and notable efficacy. The development of composite materials including graphene improves performance and expands the potential uses of regular materials. The incorporation of a minor quantity of rGO within the polymer matrix has been observed to substantially enhance the electrical and thermal conductivity of the polymer.<sup>6-8</sup> Consequently, the utilization of rGO-rubber nanocomposites can yield superior mechanical and dynamic properties compared to conventional rubber-based materials.<sup>9</sup>

Although there are considerable number of publications on rGO/polymer composites limited work has been done on, graphene-based rubber composites. Moreover, these studies are limited to primary characterization and not explored detailed property investigation. The present study focuses on detailed investigation of mechanical and electrical properties of rGO/rubber nanocomposite in which rGO has been prepared using high purity vein graphite.

## Materials and Methods

### Materials

Natural graphite with 99% carbon was supplied by the Ragedera mine. Rubber Latex (NR) compounded natural rubber (CNR), coagulants, dispersing agents, and vulcanized agents obtained from the local rubber industry were used as received.  $H_2SO_4$ ,  $KMnO_4$ ,  $H_2O_2$ , HCl,  $BaCl_2$  and acetic acid are in analytical grade.

### Synthesis of Reduced Graphene Oxide

Graphene oxide was synthesized using natural graphite through the modified Hummer's method.<sup>10, 11</sup> 1.0g of graphite was added to 20cm<sup>3</sup> of conc.  $H_2SO_4$  at 0°C and 3.0 g of  $KMnO_4$  was gradually added to the mixture while stirring. The mixture was stirred at room temperature for 30 min and 50 cm<sup>3</sup> of water was added slowly. Over again, 150 cm<sup>3</sup> of distilled water followed by 10 cm<sup>3</sup> of 30%  $H_2O_2$  solution were added. The solids were separated by centrifuging and repeatedly washing with 5% HCl until sulfate was not detected with  $BaCl_2$ . The product was washed with acetone and dried in an oven at 60°C overnight to obtain graphite oxide (GO). The resulting GO was reduced

by heating at 250°C in air for 5–10 min to obtain reduced graphene oxide, rGO.<sup>12, 10</sup>

### Preparation of Reduced Graphene Oxide/Rubber Nanocomposite

At first, rGO dispersion was prepared by well mixing rGO in water. While stirring the mixture NR latex and polymeric dispersant agent is added to form a nanocomposite.<sup>13</sup> The mixture was coagulated using acetic acid. The excess moisture in the mixture was removed by drying in an oven at 105°C. Dry sheets were subsequently vulcanized with sulfur to obtain the final rGO-NR rubber nanocomposite for characterization. A series of rGO-rubber nanocomposites were prepared by changing the rGO percentage according to the DRC of the NR latex.

### Material Characterization

To identify the crystalline phase composition of the rGO-rubber composite, X-ray powder diffraction (XRD) analysis was performed. For this analysis, the Regaku Ultima IV X-ray diffractometer equipped with Cu K $\alpha$  radiation ( $\lambda = 1.5406 \text{ \AA}$ ) was employed. The instrument operated at a voltage of 40kV and a current of 40mA. A LEO 1420vp scanning electron microscope (SEM) was utilized to examine the morphology of the composite material. To confirm the formation of rGO, natural rubber, and rGO-rubber composites, Fourier Transform Infrared Spectroscopy (FTIR) characterization was carried out using a BRUKER Tenor 27 FTIR-ATR spectrometer. The electrical resistivity of the composite was measured using a two-point probe method. The hardness and the tensile properties of the composite were measured according to ISO standards.

## Results and Discussion

### X-Ray Diffraction (XRD) Analysis

In Figure 1, the XRD spectra of graphite oxide (GO) and reduced graphene oxide (rGO) derived from natural graphite are depicted. The presence of a highly intense and sharp peak at approximately  $2\theta = 11^\circ$  in Figure 1(a) confirms the successful formation of GO from natural graphite.<sup>11, 12</sup> Subsequently, a thermal treatment was followed to reduce GO and formation of rGO.<sup>13, 14</sup> The disappearance of the peak at  $2\theta = 11^\circ$  in GO and the appearance of a new broad peak at approximately  $2\theta = 26^\circ$  in Figure 1(b) provide

further evidence for the complete transformation of GO into rGO.<sup>14</sup>

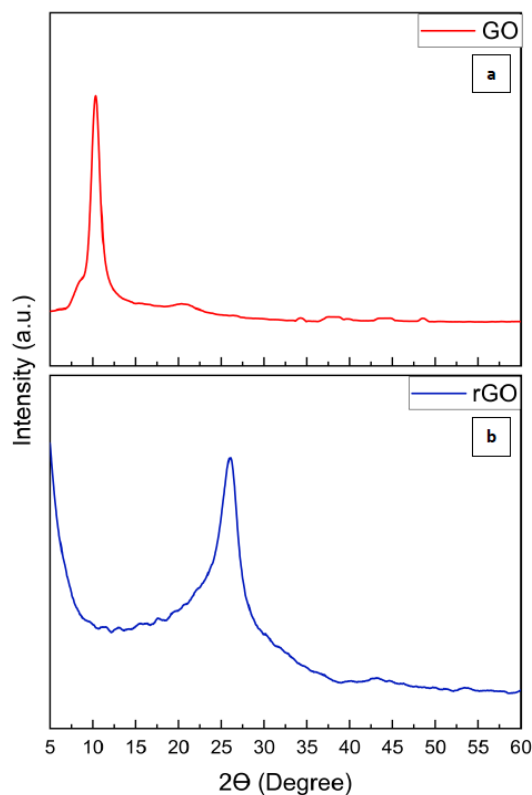


**Fig.1: XRD spectrum of (a) graphite oxide(GO) and (b) reduced graphene oxide (rGO)**

The reduction process of GO to produce rGO resulted in the removal of a significant portion of oxygen-containing functional groups. The effectiveness of this reduction process was confirmed by the reduction in the d-spacing of GO from 0.97 nm to 0.36 nm, which corresponds to the d-spacing of rGO.<sup>15</sup> Additionally, the presence of broad peaks at the 002 reflection for rGO indicates that the crystal phase of rGO was randomly arranged in comparison to the highly crystalline structure of natural graphite. The presence of a border peak in the spectrum at approximately  $2\theta = 26^\circ$ , resembling that of graphite, provides further confirmation that the  $\pi$ -conjugated graphene structure was notably restored during the preparation process of rGO.<sup>16</sup>

The main XRD peak of graphite for 002 plane generally appears at  $2\theta \sim 26^\circ$  and the corresponding

d-spacing is  $\sim 0.33$  nm<sup>17</sup>. Another peak with less intensity is observed at  $2\theta = 42.60^\circ$  with 001 orientation. This peak was formed due to the turbostratic band of disordered carbon materials.<sup>18</sup> Figure 2 illustrates the XRD spectrum of rGO-rubber nanocomposites at 1%, 2%, and 3% rGO in rubber. All patterns exhibit the characteristics peak of natural rubber at about  $2\theta = 19^\circ$ .<sup>19</sup> However, the characteristic peak of rGO is not prominent, presumably due to overlapping of the graphite peak by the broad peak corresponding to rubber.

### Scanning Electron Microscopy (SEM)

Figure 3 presents scanning electron microscope (SEM) images of the rGO rubber nanocomposite captured at various magnifications. Figures 3 (a) and (b) reveal the presence of rGO particles embedded within the surface of the compounded natural rubber (CNR). However, it was noted that the dispersion of rGO particles within the polymer matrix was not uniform. This observation was particularly evident in the cross-section of the rGO/rubber nanocomposite as shown in Figure 4.

In Figure 4 (a), it can be observed that most of the rGO particles are embedded within the polymer matrix as a result of the heating process. On top of the nanocomposite sheet, a thin layer of CNR is visible. This occurrence can be attributed to the high-

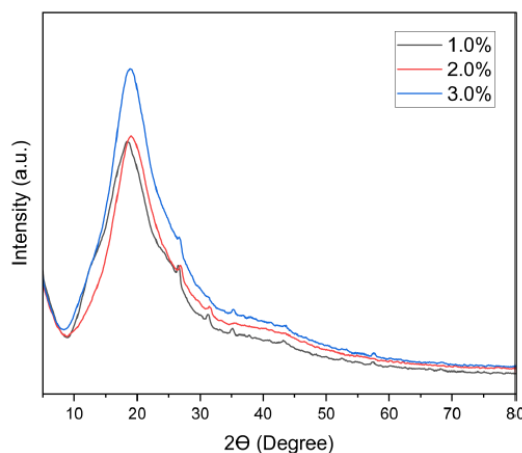


**Fig.2: XRD Spectrums of rGO-CNR nanocomposites at 1% rGO, 2% rGO and 3% rGO**

water content in the rGO dispersion. The presence of water reduces the density of CNR in the rGO/rubber nanocomposite, leading to the precipitation of rGO particles at the bottom due to the force of gravity. Consequently, non-homogeneity is observed in the composite. The precipitation of rGO becomes more prominent at lower percentages of rGO in rubber, while the homogeneity of the composite improves with an increase in the amount of rGO in rubber.

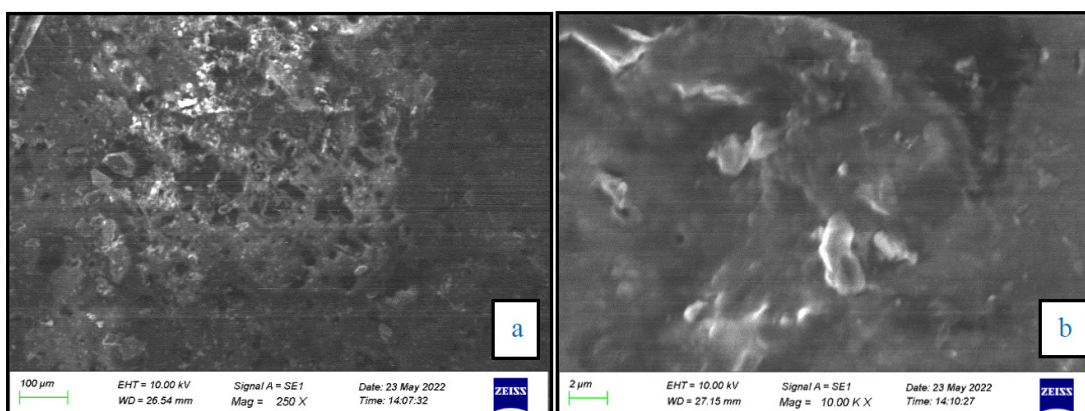


**Fig.3: SEM image of rGO/rubber nanocomposite at (a) x250 and (b) x10k**

**Fourier Transform Infrared Spectroscopy (FTIR)** FTIR spectroscopy, utilizing the ATR (Attenuated Total Reflectance) technique, was employed to identify and confirm the functional groups present in the samples. Figure 5 illustrates the FTIR spectrum

of rGO and dispersed rGO. The peak observed at  $1556\text{ cm}^{-1}$  corresponds to the C-C skeleton vibration of rGO, which remains even after the dispersion of rGO and indicates the chemical inertness of the bulk rGO. Additionally, a highly intense band at  $3155$

$\text{cm}^{-1}$  is attributed to the O-H stretching vibration, confirming the presence of O-H functional groups within the structure.<sup>20</sup> The FTIR analysis of rGO before and after dispersion confirmed the absence

of significant functional groups or changes in the rGO structure upon dispersion. This suggests that the structure of rGO remains mostly unchanged after the dispersion process.

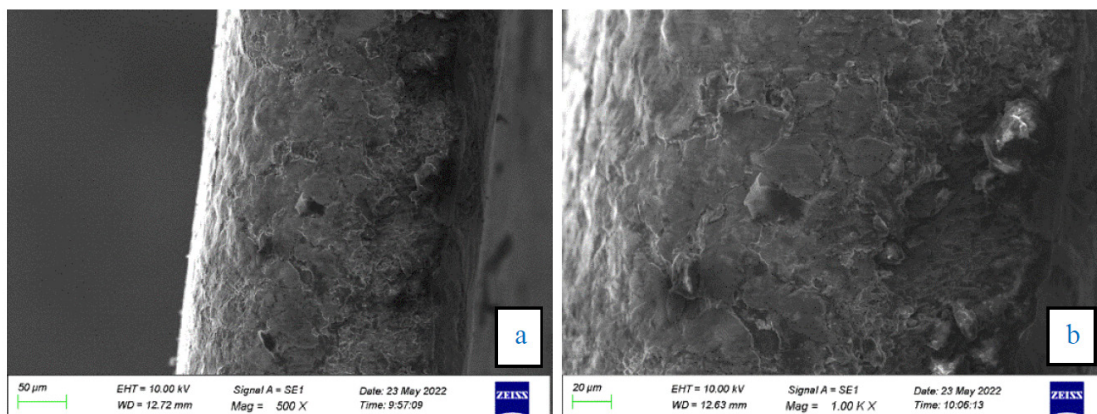


**Fig.4: SEM image of the cross-section of rGO/rubber nanocomposite at (a)x500 and (b)x1k**

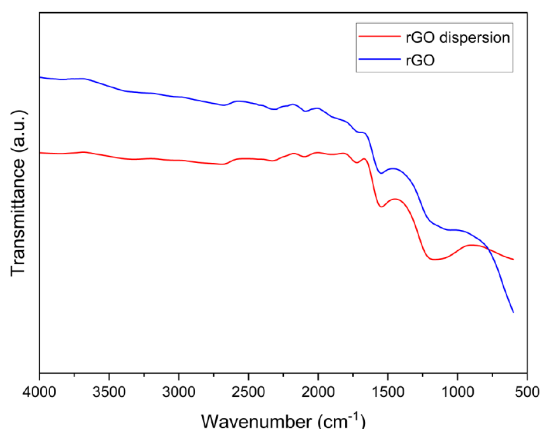


**Fig. 5: FTIR Spectrum of rGO & rGO dispersion**

Figure 6 presents the FTIR spectra of rGO, CNR, and a 3.0% rGO/rubber nanocomposite. Upon comparison with the FTIR spectrum of CNR, identical peaks corresponding to CNR can be observed in the 3.0% rGO/rubber nanocomposite. Notably, the peak at approximately 3330  $\text{cm}^{-1}$ , corresponding to the stretching vibration of the N-H group present in the amide group, is present. Additionally, peaks corresponding to the asymmetrical stretching of the methyl group ( $-\text{CH}_3$ ) at 2960  $\text{cm}^{-1}$ , the scissoring vibration of the  $-\text{CH}_2$  band at around 2917  $\text{cm}^{-1}$ , and the out-of-plane bending of the C=C bond (cis -1,4 unit) at 832.2  $\text{cm}^{-1}$  are also observed in the nanocomposite without significant changes.<sup>21</sup>

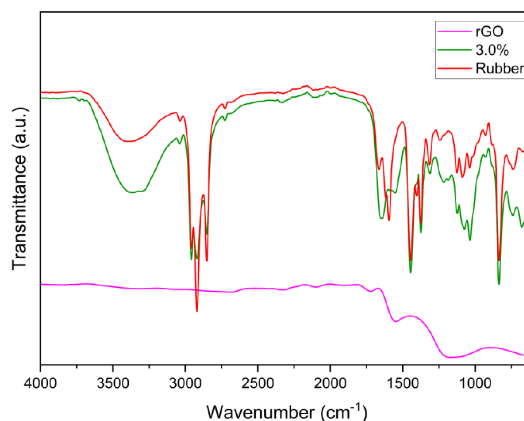


**Fig. 6: FTIR Spectrum of rGO, CNR & 3.0% rGO/NR Nanocomposite**

These characteristic peaks confirmed that the functionalities of CNR remain unchanged in the 0.5% rGO/rubber nanocomposite. Additionally, slight visibility of identical peaks for rGO in the FTIR spectrum of the 3.0% rGO/rubber nanocomposite indicates that the functionalities of rGO also remain unchanged in the final composite.

Figure 7 depicts the FTIR spectra of rGO-CNR nanocomposites with varying rGO ratios ranging from 0.5% to 3.0%. The spectra show clear and identical peaks for both compounded natural rubber and reduced graphene oxide. However, the

intensities of these identical peaks corresponding to CNR gradually decrease as the rGO ratio in the nanocomposite increases. This suggests that the presence of rGO influences the intensities of these peaks, indicating the influence of rGO on the CNR component of the nanocomposite.

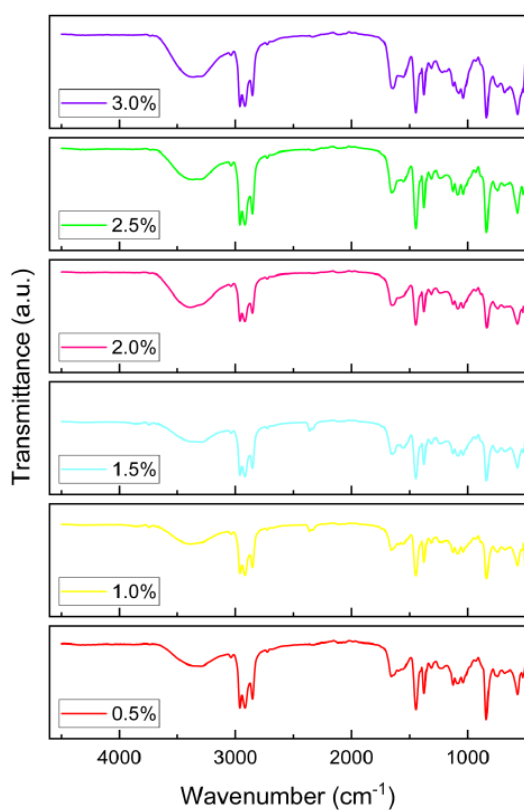


**Fig. 7: FTIR Spectrum of rGO/NR nanocomposites varies with the rGO percentage**

### Electrical Conductivity

The electrical conductivity of the rGO/rubber nanocomposite was measured using two probe methods. Table 1 indicates the measured resistance and the calculated conductivity of the rGO/rubber nanocomposites at different rGO content. The conductivity of the nanocomposite was significantly increased with increasing rGO in the rubber. The electrical conductivity is shown only at the bottom surface of the nanocomposite sheet at 1.0% and 1.5% rGO due to precipitation of rGO in the bottom at lower density of rGO. The top surface of the composite sheet is covered with a low-density CNR layer, acting as an electrical insulator. However, at

2%, 2.5%, and 3% rGO in the composite results in a homogeneous distribution of rGO in the polymer matrix and sufficiently occupied throughout the rubber matrix resulting in a higher conductivity in the overall composite sheet.

**Table 1: Resistance and Conductivity of rGO/ rubber Nanocomposite**

| Sample | Resistance ( $\Omega$ ) | Conductivity ( $\text{Sm}^{-1}$ ) |
|--------|-------------------------|-----------------------------------|
| 0.5    | $\infty$                | 0                                 |
| 1.0    | 500k                    | 0.04                              |
| 1.5    | 100k                    | 0.20                              |
| 2.0    | 50k                     | 0.40                              |
| 2.5    | 32k                     | 0.62                              |
| 3.0    | 26k                     | 0.77                              |

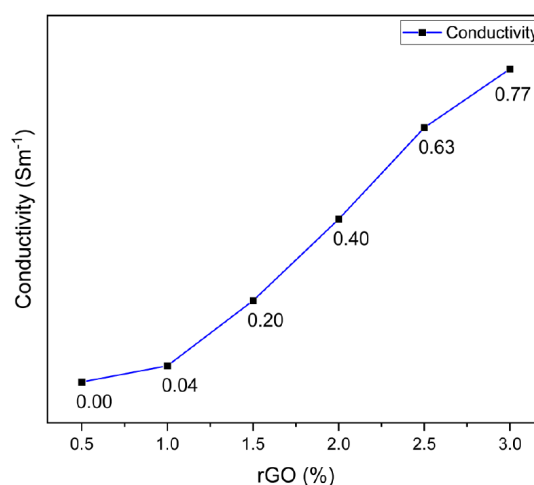


**Fig. 8: Variation in conductivity of rGO/rubber nanocomposite with rGO ratio**

Figure 8 illustrates the conductivity variation with respect to the rGO ratios. The electrical conductivity of the nanocomposite was observed to be directly related to the rGO percentage. According to the regression line of the graph in Figure 8, the regression equation for the electrical conductivity of the resultant composite was  $\hat{y} = 0.33143X - 0.241$ . Therefore, the electrical conductivity of the rGO/rubber nanocomposite exhibits " $\hat{y} = bX + a$ " model variation with the rGO percentage. Particles of rGO in the nanocomposite begin to contact each other with increasing rGO, creating conductive paths throughout the sheet.

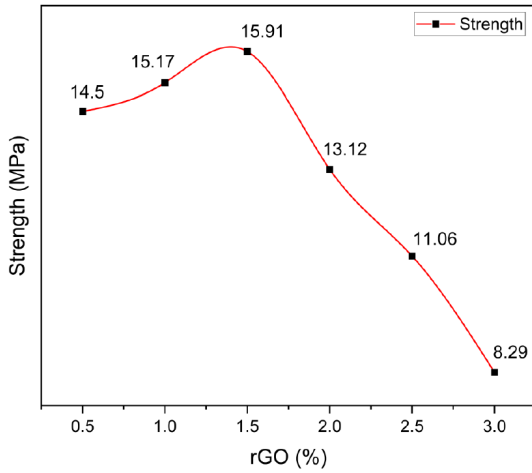


**Fig. 9: Variation of the strength of rGO/rubber nanocomposite with rGO percentage**

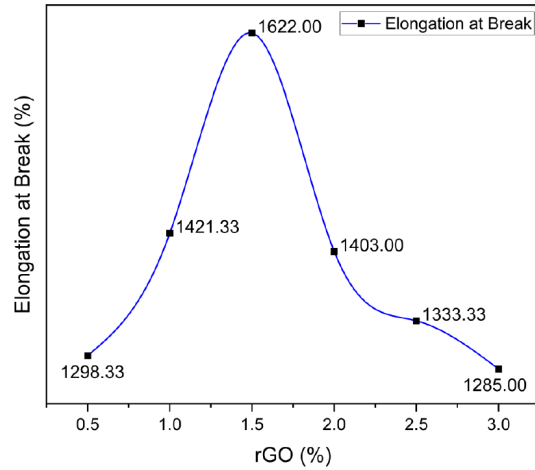


**Fig. 10: Variation of Elongation at break of rGO/rubber nanocomposite with rGO percentage**

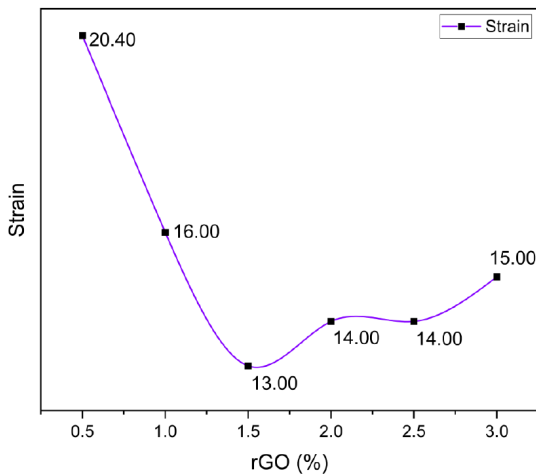


**Fig. 11: Variation of the strain of rGO/rubber nanocomposite with rGO percentage**

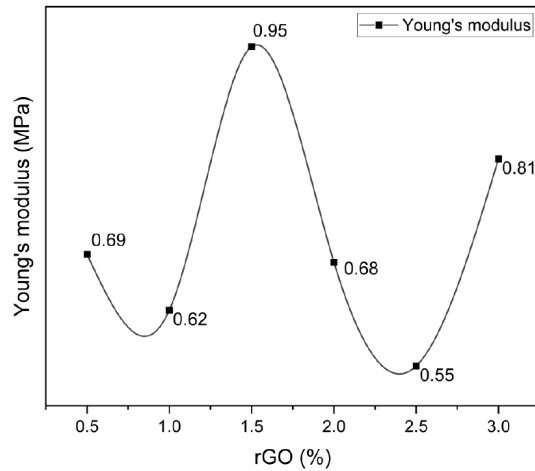


**Fig. 12: Variation of Young's modulus of rGO/rubber nanocomposite with rGO percentage**

**Mechanical Property Analysis**

Strength, Elongation at break, Strain, Young's Modulus, and hardness of the rGO/rubber nanocomposite were measured to analyze the mechanical properties of the NR/Rubber nanocomposite. Figures 9 to 13 illustrate the changes in mechanical properties as a function of the rGO percentage in the nanocomposite. These figures demonstrate the relationship between the rGO content and various mechanical properties, providing valuable insights into the impact of rGO on the overall performance of the nanocomposite. The overall strength of the nanocomposite was

gradually increased by increasing the rGO ratio up to 1.5% , as displayed in Figure 9. The maximum tensile strength was observed at 1.5% rGO as 15.91 MPa. Thereafter, the strength rapidly decreased even below the original strength of the CNR. The nanocomposite with 1.5% rGO is better reinforced compared with other samples, and higher strength than the control sample was observed for composites containing 0.5%, 1.0% and 1.5% rGO. The deformation degree of the molecular rubber chains under stress was restricted by the rGO particles in the composite. The tensile strength was highly dependent on the energy that required

for the deformation and fracturing of the polymer chains. The addition of rGO to the rubber matrix increases the polymer–filler interactions and leads to an increase in the effective cross-link density of the resulting composite. As a result, the strength of the composite was increased. However, the strength of the composite started to decrease subsequently due to the lack of pure latex content compared to rGO content.

The variation of elongation at break (%) with rGO percentage (%) for rGO/rubber nanocomposite was shown in Figure 10. According to the results, elongation at the break of the composite was increased with the rGO percentage until 1.5% of rGO and decreased again with the rGO percentage. The maximum elongation at break was reported for 1.5% of rGO/rubber nanocomposite as 1622. The nanocomposite with 1.5% rGO was the only sample that exhibited higher elongation at break than the control sample.

The graph of the strain of rGO/rubber nanocomposite vs rGO percentage is illustrated in Figure 11. The strain of the nanocomposite was rapidly decreased until 1.5% of rGO in the composite. After that strain of the composite was gradually increased below the reference sample. Therefore, the addition of rGO to the rubber matrix caused a reduction in strain of the resultant composite. The interactions between rGO particles and the rubber matrix caused a restriction in the movement of the polymer chains in the composite. The lowest strain value was reported for the 1.5% of rGO in nanocomposite.

The variation of Young's modulus of rGO/rubber nanocomposite with the rGO percentage is shown in Figure 12. Young's modulus of the composite was gradually decreased until 1% of rGO and rapidly increased up to the highest reported value in this experiment, that is 0.96 MPa at 1.5%. After that, Young's modulus of the composite decreased again gradually, but 3% of rGO in rubber composite shows a significant increase in Young's modulus. 1.5 % and 3.0% of rGO in rubber were the only ratios that exhibited higher Young's modulus than that of the control CNR sample.

The variation of the hardness of rGO/ rubber nanocomposite with the rGO percentage was illustrated in Figure 13. Compared to the other

properties, the hardness of the nanocomposite exhibited significantly different variations. According to the test results, the hardness of the composite was continuously increased with an increasing rGO percentage, and the highest value was reported with a 3% rGO. Therefore, further addition of rGO to the rubber matrix causes an increase in the hardness of the final composite.

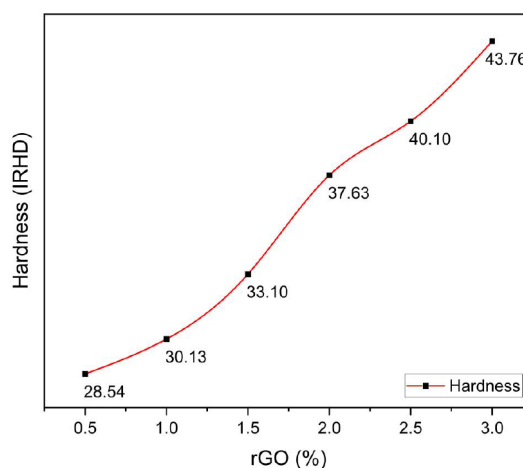


**Fig. 13: Variation of the hardness of rGO/ rubber nanocomposite with rGO percentage**

## Conclusions

The investigation of optimal electrical and mechanical properties in rGO-rubber nanocomposites has yielded significant findings with direct practical applications. The successful preparation of varying nanocomposites demonstrated effective and uniform dispersion of reduced graphene oxide (rGO) within the natural rubber matrix, ensuring minimal loss or wastage. The nanocomposites exhibited their highest tensile strength, Young's modulus, elongation at break, and lowest strain at an rGO content of 1.5% in natural rubber. Moreover, increasing the rGO percentage led to improved hardness, while the addition of rGO resulted in a remarkable enhancement of electrical conductivity. This research represents a noteworthy advancement by independently optimizing the mechanical and electrical properties, making a valuable contribution to the field. The use of pure Sri Lankan graphite for rGO synthesis adds more value to the local graphite industry and enables direct industrial applicability of rGO-rubber nanocomposites. Nonetheless, the established optimum rGO percentages for individual properties have significant practical implications

for future product development, differentiating this research from prior studies. These findings offer valuable insights for informed decision-making in material design and development, particularly for industries seeking to capitalize on the benefits of rGO-rubber nanocomposites. The key contributions of this research lie in the application of an industrially feasible synthesis method at optimized conditions. Despite the interchanges between properties, these findings offer practical insights for product development and propel advancements in the field of rGO-based nanocomposites, fostering opportunities for innovative applications.

#### Acknowledgements

The financial support is provided by National Research Council (NRC Grant No. 16/138).

#### Funding

The author(s) received no financial support for the research, authorship, and/or publication of this article.

#### Conflict of interest

There is no conflict of interest regarding the publication of this article.

#### References

1. T. Kurian and N. M. Mathew, "Natural Rubber: Production, Properties and Applications," in *Biopolymers: Biomedical and Environmental Applications*, 2011. doi: 10.1002/9781118164792.ch14.
2. P. Posadas, A. González-Jiménez, and J. L. Valentín, "Natural rubber: Properties, behavior and uses," in *Natural Rubber: Properties, Behavior and Applications*, 2016.
3. S. Kohjiya and Y. Ikeda, *Chemistry, manufacture and applications of natural rubber*. 2014. doi: 10.1533/9780857096913.
4. A. A. Vozniakovskii, A. P. Vozniakovskii, S. v. Kidalov, J. Otvalko, and A. Yu Neverovskaia, "Characteristics and mechanical properties of composites based on nitrile butadiene rubber using graphene nanoplatelets," *J Compos Mater*, vol. 54, no. 23, 2020, doi: 10.1177/0021998320914366.
5. S. Songsaeng, P. Thamyongkit, and S. Poompradub, "Natural rubber/reduced-graphene oxide composite materials: Morphological and oil adsorption properties for treatment of oil spills," *J Adv Res*, vol. 20, 2019, doi: 10.1016/j.jare.2019.05.007.
6. Y. J. Yang and W. Li, "CTAB functionalized graphene oxide/multiwalled carbon nanotube composite modified electrode for the simultaneous determination of ascorbic acid, dopamine, uric acid and nitrite," *Biosens Bioelectron*, vol. 56, 2014, doi: 10.1016/j.bios.2014.01.037.
7. C. Chen *et al.*, "Self-assembled free-standing graphite oxide membrane," *Advanced Materials*, vol. 21, no. 29, 2009, doi: 10.1002/adma.200803726.
8. L. D. C. Nayanajith, R. C. L. de Silva, S. R. R. S. Rosa, and I. R. M. Kottegoda, "Evaluation of Conducting and Tensile Properties of Reduced Graphene Oxide/ Polybutylene Adipate Terephthalate (Rgo/Pbat) Nanocomposites," *Material Science Research India*, vol. 19, no. 1, pp. 26–35, May 2022, doi: 10.13005/MSRI/190103.
9. H. Zhang, W. Xing, H. Li, Z. Xie, G. Huang, and J. Wu, "Fundamental researches on graphene/rubber nanocomposites," *Advanced Industrial and Engineering Polymer Research*, vol. 2, no. 1. 2019. doi: 10.1016/j.aiepr.2019.01.001.
10. A. M. K. L. Abeykoon, R. C. L. De Silva, L. D. C. Nayanajith, and I. R. M. Kottegoda, "A review on appropriate graphene synthesis methods for diverse applications," *Sri Lankan Journal of Physics*, vol. 23, no. 2, p. 125, Dec. 2022, doi: 10.4038/SLJP.V23I2.8116.
11. I. R. M. Kottegoda, N. H. Idris, L. Lu, J. Z. Wang, and H. K. Liu, "Synthesis and characterization of graphene-nickel oxide nanostructures for fast charge-discharge application," *Faculty of Engineering - Papers (Archive)*, vol. 56, no. 16, p. 5815, Jan. 2011, doi: 10.1016/j.electacta.2011.03.143.
12. M. T. V. P. Jayaweera, R. C. L. De Silva, I. R. M. Kottegoda, and S. R. D. Rosa, "Synthesis, characterization and ethanol vapor sensing performance of SnO<sub>2</sub>/Graphene composite

- film," *Sri Lankan Journal of Physics*, vol. 15, no. 0, p. 1, Jan. 2015, doi: 10.4038/SLJP.V15I0.6345.
13. V. Jayaweera, W. L. N. C. Liyanage, R. C. L. De Silva, S. R. D. Rosa, and I. R. M. Kottegoda, "Reduced Graphene Oxide-sno2-Polyaniline Ternary Composite for High-Performance Supercapacitors," *Material Science Research India*, vol. 18, no. 2, pp. 206–216, Aug. 2021, doi: 10.13005/MSRI/180208.
  14. I. R. M. Kottegoda *et al.*, "Comparison of Few-layer Graphene Prepared from Natural Graphite through Fast Synthesis Approach," *J Mater Sci Technol*, vol. 31, no. 9, pp. 907–912, Sep. 2015, doi: 10.1016/j.jmst.2015.07.014.
  15. D. Hou *et al.*, "Facile synthesis of graphene via reduction of graphene oxide by artemisinin in ethanol," *Journal of Materiomics*, vol. 4, no. 3, pp. 256–265, Sep. 2018, doi: 10.1016/J.JMAT.2018.01.002.
  16. N. M. S. Hidayah *et al.*, "Comparison on graphite, graphene oxide and reduced graphene oxide: Synthesis and characterization," *AIP Conf Proc*, vol. 1892, Oct. 2017, doi: 10.1063/1.5005764.
  17. A. M. Golsheikh, N. M. Huang, H. N. Lim, and R. Zakaria, "One-pot sonochemical synthesis of reduced graphene oxide uniformly decorated with ultrafine silver nanoparticles for non-enzymatic detection of H<sub>2</sub>O<sub>2</sub> and optical detection of mercury ions," *RSC Adv*, vol. 4, no. 69, pp. 36401–36411, 2014, doi: 10.1039/C4RA05998K.
  18. M. S. Seehra, V. Narang, U. K. Geddam, and A. B. Stefaniak, "Correlation between X-ray diffraction and Raman spectra of 16 commercial graphene—based materials and their resulting classification," *Carbon N Y*, vol. 111, p. 380, Jan. 2017, doi: 10.1016/J.CARBON.2016.10.010.
  19. J. Johns and V. Rao, "Characterization of natural rubber latex/chitosan blends," *International Journal of Polymer Analysis and Characterization*, vol. 13, no. 4, pp. 280–291, Jul. 2008, doi: 10.1080/10236660802190104.
  20. "Szabo, T., Berkesi, O. and Dekany, I. (2005) DRIFT Study of Deuterium-Exchanged Graphite Oxide. Carbon, 43, 3186-3189. - References - Scientific Research Publishing." [https://www.scirp.org/\(S\(351jmbntvnsjt1aadkozje\)\)/reference/referencespapers.aspx?referenceid=1531069](https://www.scirp.org/(S(351jmbntvnsjt1aadkozje))/reference/referencespapers.aspx?referenceid=1531069) (accessed May 16, 2023).
  21. R. Lu, W. Gan, B. H. Wu, Z. Zhang, Y. Guo, and H. F. Wang, "C-H stretching vibrations of methyl, methylene and methine groups at the vapor/Alcohol (n = 1-8) interfaces," *Journal of Physical Chemistry B*, vol. 109, no. 29, pp. 14118–14129, Jul. 2005, doi: 10.1021/JP051565Q.